J|A|C|S
ARTICLES
Published on Web 09/04/2003

Gas-Phase Ion Mobilities and Structures of Benzene Cluster Cations $(C_6H_6)_n^+$, $n = 2-6$

Mark J. Rusyniak, Yehia M. Ibrahim, Douglas L. Wright, Shiv N. Khanna,† and M. Samy El-Shall*

Contribution from the Department of Chemistry, Virginia Commonwealth University, Richmond, Virginia 23284-2006

Received April 7, 2003; E-mail: selshall@hsc.vcu.edu

Abstract: Benzene clusters are generated by pulsed supersonic beam expansion, ionized by electron impact, mass-selected and then injected into a drift cell for ion mobility measurements in a helium buffer gas. The measured collision cross sections and theoretical calculations are used to determine the structures of the cluster cations $(C_6H_6)_n^+$ with $n = 2-6$. Density functional theory calculation, at an all-electron level and without any symmetry constraint, predicts that the dimer cation has two nearly degenerate ground state structures with the sandwich configuration more stable than the T-configuration by only 0.07 eV. The ion mobility experiment indicates that only one structure is observed for the mass-selected dimer cation at room temperature. The calculated cross section for the sandwich structure agrees very well (within 2.4%) with the experimental value. For the $n = 3-6$ clusters, the experiments suggest the presence of at least two structural isomers for each cluster. A Monte Carlo minimum-energy search technique using the 12-site OPLS potential for benzene is used to determine the structures of the lowest-energy isomers. The calculated cross sections for the two lowest-energy isomers of the $n = 3-6$ clusters agree well with the experimental results. The clusters' structures reveal two different growth patterns involving a sandwich dimer core or a pancake trimer stack core. The lowest-energy isomers of the $n = 3-6$ clusters incorporate the pancake trimer stack as the cluster's core. The trimer stack allows the charge to hop between two dimers, thus maximizing charge resonance interaction in the clusters. For larger clusters, the appearance of magic numbers at $n = 14$, 20, 24, 27, and 30 is consistent with the incorporation of a sandwich dimer cation within icosahedral, double icosahedral, and interpenetrating icosahedral structures. On the basis of the ion mobility results and the structural calculations, the parallel-stacked motif among charged aromatic−aromatic interactions is expected to play a major role in determining the structures of multi aromatic components. This conclusion may provide new insights for experimental and theoretical studies of molecular design and recognition involving aromatic systems.

I. Introduction

The study of molecular cluster ions is an active area of research in the rapidly advancing field of cluster science.[1−3] These studies are motivated by many objectives including fundamental understandings of intermolecular and ion−molecule interactions as well as molecular level insights into condensed-phase processes such as ion solvation and ion-induced nucleation. Gas-phase clusters provide good models for these processes since the size effect, and the degree of complexity of the interaction can be systematically varied in well-defined systems.[1−5]

Because of the differences in the geometry and binding energy of the neutral and the ionized cluster, the cluster ion produced is often intermolecularly vibrationally excited. Energy transfer to the low-frequency cluster modes leading to evaporation can dissipate the excess energy resulting from the relaxation process upon ionization. In this way, structural isomers can be stabilized within the cluster by evaporative cooling which is analogous to collisional stabilization of the ionic intermediates in the gas phase at high pressures. In addition, the cluster environment permits some unique cooperative effects such as those involving three-body interactions, which are generally very inefficient in the gas phase, particularly at low pressures.[1−5]

Benzene clusters provide the simplest prototype system to study $\pi-\pi$ interactions which are of fundamental interest in many areas of chemistry and biology including, for example, protein structures, DNA, host−guest complexes, and self-assembled architectures.[6−10] An extensive amount of work has been devoted to the spectroscopy and structure of neutral benzene clusters synthesized in supersonic jets and probed by fluorescence excitation, resonance-enhanced multiphoton ioniza-

† Department of Physics, Virginia Commonwealth University.

(1) Castleman, A. W., Jr.; Wei, S. *Annu. Rev. Phys. Chem.* **1994**, *45*, 685.
(2) Castleman, A. W., Jr.; Bowen, K., Jr. *J. Phys. Chem.* **1996**, *100*, 12911.
(3) Duncan, M. A. *Annu. Rev. Phys. Chem.* **1997**, *48*, 69.
(4) Armentrout, P. B. *Annu. Rev. Phys. Chem.* **2001**, *52*, 423.
(5) Buck, U. *J. Phys. Chem.* **2002**, *106*, 10049.
(6) Burley, S. K.; Petsko, G. A. *Science* **1985**, *229*, 23.
(7) Smithrud, D. B.; Diederich, F. *J. Am. Chem. Soc.* **1990**, *112*, 339.
(8) Rebek, J., Jr. *Chem. Soc. Rev.* **1996**, *25*, 255.
(9) Hunter, C. A.; Sanders, J. K. M. *J. Am. Chem. Soc.* **1990**, *112*, 5525.
(10) Fyfe, M. C. T.; Stoddart, J. F. *Acc. Chem. Res.* **1997**, *10*, 393.

10.1021/ja035504m CCC: $25.00

tion, and stimulated Raman spectroscopy techniques.[11−30] Less experimental and theoretical works have been focused on the cluster cations $(C_6H_6)^+_n$ with most of published work dealing with the dimer cation.[31−44] Unlike the neutral dimer where the ground state has a perpendicular T-shaped structure,[21,45,46] it has been suggested that the dimer cation adopts a parallel sandwich configuration on the basis of maximizing the charge-transfer resonance interaction $C_6H_6^+ \cdot C_6H_6 \leftrightarrow C_6H_6 \cdot C_6H_6^+$.[31−34] The strong broad absorption extending from 690 to 1064 nm observed for benzene cluster cations has been attributed to dimer-based intervalence transition similar to the solid-state spectra of the dimer ions.[47] No direct structural information exists for larger cluster ions but photodissociation experiments indicate that the absorption bands of $(C_6H_6)_n^+$ with $n = 3-6$ exhibit essentially the same features as that of $(C_6H_6)_2^+$ suggesting the presence of a dimer ion core in the clusters.[40,42−44]

It is interesting to investigate how the addition of several benzene molecules to the dimer cation affects the structures of the clusters. It is also of interest to see if the growth sequence of the cluster cations can be related to that of the neutral clusters. On the basis of the sandwich and T-shaped dimer configurations,[21] one may consider four major structural motifs for the growth of the larger clusters. These growth patterns, as shown below, may be described as eclipsed stacked sandwich (ESS), displaced stacked parallel (DSP), eclipsed stacked T-shaped (EST), and displaced stacked T-shaped (DST).

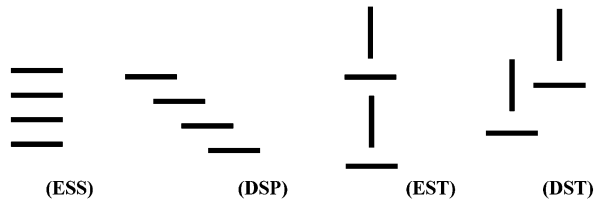

Of particular interest is the possibility of forming a stacked cluster consisting of parallel benzene rings (ESS). This structure is a good candidate for the hopping mechanism of the positive charge within the $(C_6H_6)_n^+$ cluster. In principle, the stacked cluster structure allows the charge to continually hop from one dimer to another dimer in the cluster, thus allowing all the molecules in the cluster to have equal chances of being neutral or ionic which maximizes resonance charge-transfer interaction.

In this work,, we present an experimental and theoretical study of the structures and growth pattern of benzene cluster cations $(C_6H_6)_n^+$. The experimental work utilizes the ion mobility drift cell technique. Ion mobility measurements provide an accurate method for determining collision cross sections of mass-selected ions with a buffer gas.[48−50] The motion of the ion through a buffer gas under the influence of a weak electric field depends on the ion's average collision cross section with the buffer gas.[48,49] The use of this technique to examine the structures of carbon cluster ions has sparked the recent interest in deducing structural information from mobility measurements.[51−55] Extensive work has produced novel structural information on carbon, metal, and semiconductor clusters, polymeric ions, and large polypeptide and biological molecular ions.[56−70] On the other hand, not much work has been reported on the application of ion mobility to investigate the structures of molecular cluster ions.[71−73]

(11) Hopkins, J. B.; Powers, D. E.; Smalley, R. E. *J. Phys. Chem.* **1981**, *85*, 3739.
(12) Langridge-Smith, P. R. R.; Brumbaugh, D. V.; Haynam, C. A.; Levy, D. H. *J. Phys. Chem.* **1981**, *85*, 3742.
(13) Fung, K. H.; Selzle, H. L.; Schlag, E. W. *J. Phys. Chem.* **1983**, *87*, 5113.
(14) Law, K. S.; Schauer, M.; Bernstein, E. R. *J. Chem. Phys.* **1984**, *81*, 4871.
(15) Schauer, M.; Bernstein, E. R. *J. Chem. Phys.* **1985**, *82*, 3722.
(16) Bornsen, K. O.; Selzle, H. L.; Schlag, E. W. *J. Chem. Phys.* **1986**, *85*, 1726.
(17) van de Waal, B. W. *Chem. Phys. Lett.* **1986**, *123*, 69.
(18) Easter, D. C.; El-Shall, M. S.; Hahn, M. Y.; Whetten, R. L. *Chem. Phys. Lett.* **1989**, *157*, 277.
(19) Selzle, H. L.; Krause, H.; Ernstberger, H.; Krause, H.; Schlag, E. W. *J. Phys. Chem.* **1989**, *93*, 7535.
(20) Del Mistro, G.; Stace, A. J. *J. Chem. Phys.* **1993**, *98*, 3905.
(21) Hobza, P.; Selzle, H. L.; Schlag, E. W. *Chem. Rev.* **1994**, *94*, 1767.
(22) Felker, P. M.; Maxton, P. M.; Schaeffer, M. W. *Chem. Rev.* **1994**, *94*, 1787.
(23) Maxton, P. M.; Schaeffer, M. W.; Felker, P. M. *Chem. Phys. Lett.* **1995**, *241*, 603.
(24) Easter, D. C.; Mellott, J.; Weiss, T. *J. Chem. Phys.* **1998**, *109*, 8365.
(25) Spirko, V.; Engkvist, O.; Soldan, P.; Selzle, H. L.; Schlag, E. W.; Hobza, P. *J. Chem. Phys.* **1999**, *111*, 572.
(26) Benharash, P.; Gleason, M. J.; Felker, P. M. *J. Phys. Chem. A* **1999**, *103*, 1442.
(27) Gonzalez, C.; Lim, E. C. *J. Phys. Chem. A* **2001**, *105*, 1904.
(28) Limori, T.; Ohshima, Y. *J. Chem. Phys.* **2002**, *117*, 3656.
(29) Limori, T.; Yasuhito, A.; Ohshima, Y. *J. Chem. Phys.* **2002**, *117*, 3675.
(30) Easter, D. C. *J. Phys. Chem. A* **2003**, *107*, 2148.
(31) Badger, B.; Brocklehurst, B. *Nature* **1968**, *219*, 263.
(32) Field, F. H.; Hamlet, P.; Libby, W. F. *J. Am. Chem. Soc.* **1969**, *91*, 2839.
(33) Meot-Ner (Mautner), M.; Hamlet, P.; Hunter, E. P.; Field, F. H. *J. Am. Chem. Soc.* **1978**, *100*, 5466.
(34) Chandra, A. K.; Bhanuprakash, K.; Jyoti Bhasu, V. C.; Srikanthan, D. *Mol. Phys.* **1984**, *52*, 733.
(35) Snodgrass, T. T.; Dunbar, R. C.; Bowers, M. T. *J. Phys. Chem.* **1990**, *94*, 3648.
(36) Grover, J. R.; Walters, E. A.; Hui, E. T. *J. Phys. Chem.* **1987**, *91*, 3233.
(37) Stace, A. J.; Bernard, D. M.; Crooks, J. J.; Reid, K. L. *Mol. Phys.* **1987**, *60*, 671.
(38) Hahn, M. Y.; Schriver, K. E.; Whetten, R. L. *J. Chem. Phys.* **1988**, *88*, 4242.
(39) Hiraoka, K.; Fujimaki, S.; Aruga, K. *J. Chem. Phys.* **1991**, *95*, 8413.
(40) Ohashi, K.; Nishi, N. *J. Chem. Phys.* **1991**, *95*, 4002.
(41) Beck, S. M.; Hecht, J. H. *J. Chem. Phys.* **1992**, *96*, 1975.
(42) Inokuchi, Y.; Ohashi, K.; Nishi, N. *Chem. Phys. Lett.* **1997**, *279*, 73.
(43) Nakai, Y.; Ohashi, K.; Nishi, N. *J. Phys. Chem. A* **1997**, *101*, 472.
(44) Ohashi, K.; Nishi, N. *J. Chem. Phys.* **1998**, *109*, 3971.
(45) Steed, J. M.; Dixon, T. A.; Klemperer, W. *J. Chem. Phys.* **1979**, *70*, 4940.
(46) Karlstrom, G.; Linse, P.; Wallqvist, A.; Jonsson, B. *J. Am. Chem. Soc.* **1983**, *105*, 3777.
(47) Inokuchi, Y.; Nishi, N. *J. Chem. Phys.* **2001**, *114*, 7059.
(48) McDaniel, E. W.; Mason, E. A. *The Mobility and Diffusion of Ions in Gases*; John Wiley & Sons: New York, 1973.
(49) Mason, E. A.; McDaniel, E. W. *Transport Properties of Ions in Gases*; John Wiley & Sons: New York, 1988.
(50) Kemper, P. R.; Bowers, M. T. *J. Am. Soc. Mass Spectrom.* **1990**, *1*, 197.
(51) von Helden, G.; Hsu, M. T.; Gotts, N. G.; Bowers, M. T. *J. Phys. Chem.* **1993**, *97*, 8182.
(52) von Helden, G.; Kemper, P. R.; Gotts, N. G.; Bowers, M. T. *Science* **1993**, *259*, 1300.
(53) von Helden, G.; Gotts, N. G.; Bowers, M. T. *Nature* **1993**, *363*, 60.
(54) Hunter, J.; Fye, J.; Jarrold, M. F. *J. Chem. Phys.* **1993**, *99*, 1785.
(55) Bowers, M. T. *Acc. Chem. Res.* **1994**, *27*, 324.
(56) Hunter, J. M.; Fye, J. L.; Boivin, N. M.; Jarrold, M. F. *J. Phys. Chem.* **1994**, *98*, 7440.
(57) Lee, S.; Gotts, N. G.; Von Helden, G.; Bowers, M. T. *Science* **1995**, *267*, 999.
(58) von Helden, G.; Wyttenbach, T.; Bowers, M. T. *Science* **1995**, *267*, 1483.
(59) Jarrold, M. F. *J. Phys. Chem.* **1995**, *99*, 11.
(60) Clemmer, D. E.; Jarrold, M. F. *J. Mass Spectrom.* **1997**, *32*, 577.
(61) Hoaglund, C. S.; Liu, Y.; Ellington, A. D.; Pagel, M.; Clemmer, D. E. *J. Am. Chem. Soc.* **1997**, *119*, 9051.
(62) Ho, K.-M.; Shvartsburg, A. A.; Pan, B.; Lu, Z.-Y.; Wang, C.-Z.; Wacker, J. G.; Fye, J. L.; Jarrold, M. F. *Nature* **1998**, *392*, 582.
(63) Fye, J. L.; Woenckhaus, J.; Jarrold, M. F. *J. Am. Chem. Soc.* **1998**, *120*, 1327.
(64) Jarrold, M. F. *Acc. Chem. Res.* **1999**, *32*, 360.
(65) Hudgins, R. R.; Jarrold, M. F. *J. Am. Chem. Soc.* **1999**, *121*, 3494.
(66) Jarrold, M. F. *Nature* **2000**, *407*, 26.
(67) Mao, Y.; Ratner, M. A.; Jarrold, M. F. *J. Am. Chem. Soc.* **2000**, *122*, 2950.
(68) Jarrold, M. F. *Annu. Rev. Phys. Chem.* **2000**, *51*, 179.
(69) Gidden, J.; Wyttenbach, T.; Jackson, A. T.; Scrivens, J. H.; Bowers, M. T. *J. Am. Chem. Soc.* **2000**, *122*, 4692.
(70) Gidden, J.; Bushnell, J. E.; Bowers, M. T. *J. Am. Chem. Soc.* **2001**, *123*, 5610.
(71) Krishnamurthy, M.; de Gouw, J. A.; Bierbaum, V. M.; Leone, S. R. *J. Phys. Chem.* **1996**, *100*, 14908.
(72) Krishnamurthy, M.; de Gouw, J. A.; Ding, L. N.; Bierbaum, V. M.; Leone, S. R. *J. Chem. Phys.* **1997**, *106*, 530.
(73) Midey, A. J.; Viggiano, A. A. *J. Chem. Phys.* **2001**, *114*, 6072.

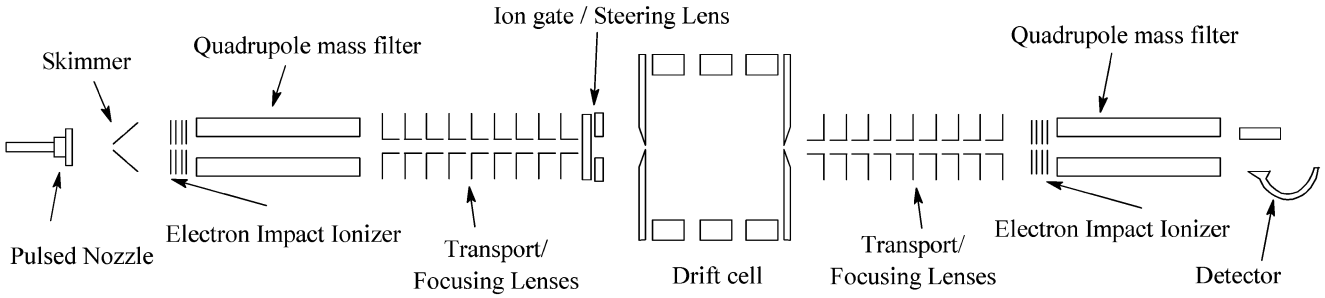

Figure 1. Experimental setup for the mass-selected ion mobility system.

The ion mobility approach requires calculations of the average collision cross sections for calculated geometries for comparison with the experimental results. For this purpose, we employ density functional theory (DFT)[74] calculations to determine the lowest-energy structures of the benzene dimer cation. Because of the nature of bonding in this system, the proper inclusion of the electron−electron correlation is essential for obtaining reliable lowest-energy structures. The use of DFT at an all-electron level in the present work ensures the accuracy of the dimer calculations in obtaining the lowest-energy structures. However, because of the size of the clusters investigated in the present study ($n = 2-6$), we employ a Monte Carlo (MC) search technique using the 12-site OPLS (*optimized potential for liquid simulation*) for the benzene molecule,[75] and a modified OPLS potential for the benzene cation to obtain minimum-energy structures. The lowest-energy structures of the $(C_6H_6)_n^+$ clusters are used to compute angle-averaged collision cross sections of the cluster cations drifting in helium. The comparison between the experimentally determined ion mobility, which depends solely on the collision cross section, and the calculated cross sections allows us to determine the structures of the benzene cluster cations involved in the current experiments. The combination of the measured ion mobilities and the structural calculations provides a reasonably compelling picture of the structure and growth pattern of the clusters of aromatic π-systems. These results are expected to provide good test models for the development of new theoretical approaches to reliably describe $\pi-\pi$ interactions in large molecular systems.

II. Experimental Section

The experimental set up for the cluster source, drift cell, and two quadrupole mass spectrometers is displayed in Figure 1. The essential elements of the apparatus are jet and beam chambers coupled to an electron impact (EI) ionization source, a quadrupole mass filter, a drift cell, and a second quadrupole mass spectrometer. A second EI ionization source is also available before the second quadrupole. This source is used to ionize the neutral cluster beam after traveling in a vacuum (in the absence of a buffer gas in the drift cell). This provides information on the original cluster ion distribution before entering the drift cell containing the helium buffer gas.

The neutral benzene clusters are generated in the source chamber by pulsed adiabatic expansion.[76,77] During operation, benzene vapor (Aldrich, 99.9% purity), in helium (ultrahigh purity, Spectra Gases 99.999%) at a pressure of 2−8 atm is expanded through a conical nozzle (200 μm diameter) in pulses of 200−300 μs duration at repetition rates of 30−50 Hz. The jet is skimmed and passed into the second chamber, which is maintained at 2×10^{-6} Torr, where the clusters are ionized by 70 eV EI ionization. The cluster ions selected by the quadrupole mass filter are focused into the drift cell for the mobility measurements as described below.

The mobility K of an ion is defined as:[48]

$$K = \vec{v}_d/\vec{E} \tag{1}$$

where $\vec{v}_d$ is the drift velocity and $\vec{E}$ the field across the drift region. The reduced mobility K_0 (scaled to the number density at standard temperature and pressure STP) is given by:

$$K_0 = \frac{P \cdot 273.15}{760 \cdot T} K \tag{2}$$

where P is the pressure in Torr and T is the temperature in Kelvin. Equations 1 and 2 can be combined and rearranged to give:

$$t_d = \left(\frac{l^2 \cdot 273.15}{T \cdot 760} \frac{1}{K_0}\right)\frac{P}{V} + t_0 \tag{3}$$

where l is the drift length (8.9 cm in our system), t_d is the measured mean arrival time of the drifting ion packet corrected for the non-Gaussian shape of the arrival time distribution (ATD) peak,[50] t_0 is the time the ion spends outside the drift cell before reaching the detector, and V is the voltage across the drift cell. All the mobility measurements were carried out in the low-field limit where the ion's drift velocity is small compared to the thermal velocity and the ion mobility is independent of the field strength ($E/N < 5.0$, where E is the electric field intensity and N is the gas number density and E/N is expressed in units of Townsend (Td) where 1 Td $= 10^{-17}$ V·cm^2).[48]

Mobility measurements are made by injecting a narrow pulse of ions into the drift cell. The ion gate located just prior to the cell entrance chops the pulse to a narrow, 5−50 μs wide packet, which enters the drift cell. As the ions are injected into the drift cell, the injection energy is dissipated in collisions with the helium buffer gas. The injection energies used in all the experiments are slightly above the minimum energies required to introduce the ions into the cell against the helium flow. The transient heating and the consequent evaporation from the cluster ions resulting from the injection energy take place outside the cell entrance through collisions with the helium escaping from the cell entrance orifice. Upon exiting the cell, the ions are collected and refocused into the second quadrupole for analysis and detection. The signal is collected on a multichannel scalar with the zero time for data acquisition set to the midpoint of the ion gate trigger. Mobility is determined according to eq 3, by plotting t_d versus P/V. The slope of the linear plot is inversely proportional to the reduced mobility, and the intercept equals the time spent within the second quadrupole before the detection of the ions. In most cases, this technique gives less than 1% standard deviation for repeated measurements.

III. Computational Details

The theoretical calcualtions were carried out using a linear combination of atomic orbital−molecular orbital (LCAO−MO) approach as implemented within a density functional formal-

(74) Kohn, W.; Sham, L. J. *Phys. Rev. A* **1965**, *140*, 1133.
(75) Jorgensen, W. L.; Severance, D. L. *J. Am. Chem. Soc.* **1990**, *112*, 4768.
(76) Daly, G. M.; Wright, D.; El-Shall, M. S. *Chem. Phys. Lett.* **2000**, *331*, 47.
(77) El-Shall, M. S.; Daly, G. M.; Wright, D. *J. Chem. Phys.* **2002**, *116*, 10253.

ism.[74] We have used, in particular, the gradient corrected functional form proposed by Perdew, Burke, and Ernzerhof.[78] The actual computations were carried out using the NRLMOL set of computer codes developed by Pederson and co-workers.[79] Here, the multicenter integrals required to solve the Kohn−Sham equation are calculated by integrating numerically over a mesh of points. To obtain the minimum-energy configuration, the geometry was relaxed by moving atoms in the directions of forces until forces were less than 10^{-4} au. Further, several multiplicities were investigated to find the ground-state spin. All the calculations were carried out at an all-electron level.

We have used the basis sets developed by Porezag and Pederson.[80] The Gaussian basis set for C contained 12 primitive Gaussians contracted into 5s, 4p, and 3d Gaussians, while the basis set for H contained eight primitive Gaussians contracted into 4s, 3p, and 1d Gaussians. To establish the accuracy of the present calculations, we first examined the ground-state geometry of neutral benzene for which the geometry and other parameters are well-known. The calculated C−C and C−H bond lengths are 1.40 and 1.09 Å compared to the experimental values of 1.406 and 1.08 Å, respectively. We find an ionization potential of 9.12 eV, which compares well with the experimental value of 9.24 eV.[81]

For the MC calculations, cluster interaction energies were calculated from site−site potentials of the form

$$\Delta e_{ab} = \sum_{i}^{ona}\sum_{j}^{onb}\left(\frac{q_i q_j e^2}{r_{ij}} + \frac{A_{ij}}{r_{ij}^{12}} - \frac{C_{ij}}{r_{ij}^{6}}\right) \qquad (4)$$

where Δe_{ab} is the interaction energy between two molecules a and b; q_i and q_j are the partial charges assigned to each atomic site i or j, and e is the magnitude of the electron charge. A_{ij} and C_{ij} can be expressed in terms of the Lennard-Jones (LJ) parameters σ and ϵ as $A_{ii} = 4\epsilon_i\sigma_i^{12}$ and $C_{ii} = 4\epsilon_i\sigma_i^{6}$, where $A_{ij} = (A_{ii}\,A_{jj})^{1/2}$ and $C_{ij} = (C_{ii}\,C_{jj})^{1/2}$ (from combining rules). The total cluster configurational energy can be expressed as $E_n = E_n^{C} + E_n^{LJ}$, where E_n^{C} is the sum of all terms representing Coulomb interactions and E_n^{LJ} the sum of all Lennard-Jones terms. For the benzene neutral, the 12-site OPLS potential was used.[75] For the benzene cation, the OPLS benzene potential was modified by altering the partial charges assigned to each site. These charges were taken from ab initio calculations at the HF/6-31G** level on the benzene cation.[82] The LJ ϵ's in the OPLS potential function for (neutral) benzene are 0.07 and 0.03 kcal/mol for carbon and hydrogen, respectively. For the cluster cation calculations, the LJ ϵ's for carbon and hydrogen were scaled up (by a factor of 23.2) to values of 1.625 and 0.6964 kcal/mol to yield a configurational energy for the dimer cation of 17.0 kcal/mol, the observed value of the binding energy of the dimer cation.[33] This enhancement of the cation−neutral interaction can be thought of as compensating for the lack of explicit treatment of the polarization of the neutral benzenes by the cation.

Cluster structures and energies were obtained through the following simulation procedure. MC simulations in the NVT ensemble were run for each cluster size using standard procedures, without truncation of the potential, and at a temperature at which no evaporation was observed.[83,84] At regular intervals during these simulations the current cluster configuration was taken as an initial structure for an auxiliary simulation resulting in a quenching of all kinetic energy from the cluster, settling it into the underlying minima of the potential energy surface. These "quenches" are begun by first expanding the cluster by scaling the center-of-mass coordinates and then giving each molecule a rather large random displacement (up to 15 Å) and rotation (up to 180°). The resulting random configuration is then allowed to settle into the underlying minima by making the usual small random displacements and rotations and accepting only those new configurations that lower the potential energy. Eventually a minimum will be reached, and when 6000−15000 consecutive trial configurations fail to find a structure of lower energy, the configuration is identified as a candidate for a minimum on the surface. Subsequently, in a separate calculation, each candidate is run at 10^{-12} K to confirm that a minimum has in fact been found and to be sure that the bottom of the well has been reached. For each cluster composition $(C_6H_6)_n$ and $(C_6H_6)_n^+$, 600−1100 quenches were performed, except for $n = 2$ where only 100 were done.

A measure of cluster radius is given by the root-mean-square distance between the molecules, given by:[85]

$$R_N = \left\langle\left(\sum_{i}^{N-1}\sum_{j>i}^{N}\frac{r_{ij}^{\,2}}{N(N-1)}\right)^{1/2}\right\rangle \qquad (5)$$

The intermolecular distances, r_{ij}, were taken as the separations of the molecular centers-of-mass, and N is the number of molecules in the cluster. This is useful for accessing the degree of compactness of clusters.

IV. Results and Discussion

1. Mass Spectra of Benzene Cluster Cations. Figure 2 displays a typical mass spectrum obtained by 70 eV EI ionization of the neutral clusters formed by a supersonic beam expansion. In this case, the neutral cluster beam traveled in a vacuum (10^{-7} Torr with no buffer gas inside the drift tube) to the second EI ionization source before the second quadrupole (see Figure 1). The mass spectrum shows the generation of doubly charged benzene clusters $(C_6H_6)_n^{2+}$ starting at $n \geq 23$. This is consistent with previous measurements and with the calculation of the critical size for doubly charged benzene clusters as $n = 23$.[37,38,86]

The distribution of the cluster ions formed reveals some striking features which include the enhanced intensities (magic numbers) observed for the $(C_6H_6)_n^+$ with $n = 14$, 20, 24, 27, and 30. These local maxima are also present at lower EI energies where no doubly charged clusters are formed, and therefore they most likely represent some stable structures among the $(C_6H_6)_n^+$ series. Following EI ionization, the excess deposited energies on the cluster ions promote evaporation of neutral molecules

(78) Perdew, J. P.; Burke, K.; Ernzerhof, M. *Phys. Rev. Lett*. **1996**, *77*, 3865.
(79) Jackson, K. A.; Pederson, M. R. *Phys. Rev. B* **1990**, *42*, 3276.
(80) Porezag, D. V.; Pederson, M. R. *Phys. Rev. A* **1999**, *60*, 2840.
(81) Neuhauser, R. G.; Siglow, K.; Neusser, H. J. *J. Chem. Phys*. **1997**, *106*, 896.
(82) The ab initio calculations were carried out at the HF/6-31G** level using the *GAMESS QC package*: Schmidt, M. W.; Baldridge, K. K.; Boatz, J. A.; Elbert, S. T.; Gordon, M. S.; Jensen, J. J.; Koseki, S.; Matsunaga, N.; Nguyen, K. A.; Su, S.; Windus, T. L.; Dupuis, M.; Montgomery, J. A. *J. Comput. Chem*. **1993**, *14*, 1347.
(83) Wright, D.; El-Shall, M. S. *J. Chem. Phys*. **1994**, *100*, 379.
(84) Wright, D.; El-Shall, M. S. *J. Chem. Phys*. **1996**, *105*, 11199.
(85) Gregory, V. P.; Schug, J. C. *Mol. Phys*. **1993**, *78*, 407.
(86) Echt, O.; Kreisle, D.; Recknagel, E.; Saenz, J. J.; Casero, R.; Soler, J. M. *Phys. Rev. A* **1988**, *38*, 3236.

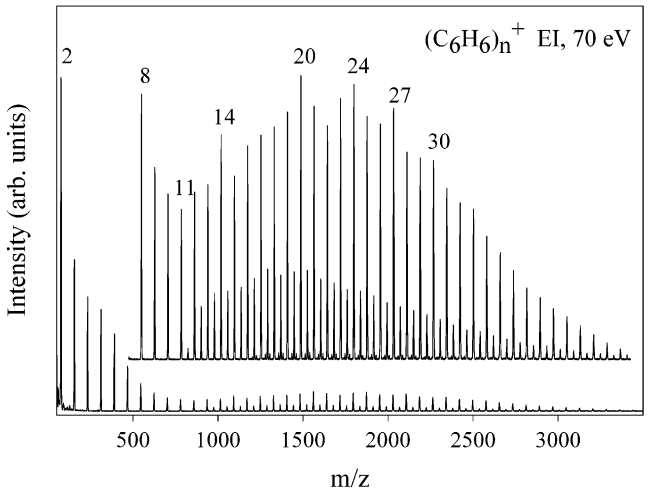

Figure 2. Mass spectrum of benzene clusters in a vacuum ionized by EI (70 eV) before the second quadrupole (see Figure 1).

from the clusters during the time spent inside the quadrupole mass filter (~50 μs). This leads to the appearance of enhanced ion intensities of specific cluster ions reflecting structural stability or particularly slow evaporation events from certain cluster ions (kinetic bottleneck).[1,2]

The $n = 13$ magic number has been first observed in atomic and small molecular clusters with LJ interactions, but has also been seen in many other cluster systems.[87−91] This magic number is attributed to an icosahedral structure, composed of a central atom or molecule covered by two staggered five-membered rings along the equator with each pole capped by another atom or molecule.[90] Extending the icosahedral symmetry by building a new icosahedron with the top apex of the 13-mer as the new center produces the $n = 19$ magic number, which is often called "double icosahedron".[90] On the basis of LJ interactions between spheres, the magic numbers 13, 19, 23, 26, 29, 32, 34, and 37 have been predicted.[91] Calculations using 12-6-1 potential functions showed that the $n = 13$ neutral clusters of several nonpolar molecules, including benzene, adopt approximate icosahedral structures.[17,92] Several computational studies suggest high-symmetry structures for the $(C_6H_6)_{13}$ neutral cluster (C_3 symmetry).[17,30,92,93]

The observation of a local maximum in the cluster ion distribution at $n = 14$ could be explained by a cluster structure consisting of a strongly bound dimer cation core surrounded by 12 neutral molecules in an icosahedral arrangement. This is consistent with previous photoionization experiments, which suggested such a structure for the $(C_6H_6)_{14}^+$ cluster[38,41] Our results provide further evidence for this structure by showing the additional local maxima of $(C_6H_6)_n^+$ observed at $n = 20$, 24, 27, and 30 (although at weaker intensities than the $n = 14$ maximum) as shown in Figure 2. These numbers are in perfect agreement with the theoretical predictions of the clustering of LJ spheres if one makes the assumption of a benzene dimer cation core within the $(C_6H_6)_n^+$ clusters. Although this assumption is appealing and provides a plausible explanation of the observed magic numbers, it lacks direct experimental evidences. The ion mobility results presented in section 4 combined with the structural calculations given in section 3 will provide the first direct evidences for the incorporation of stacked dimer and trimer cores within the benzene cluster cations with n up to 6. These core ions are expected to be present in the larger clusters which would give rise to the formation of the icosahedral structures.

2. Structural Calculations of Benzene Dimer Cation. The ground-state geometry of $(C_6H_6)_2^+$, has been thought to be a sandwich structure. The earlier electron spin resonance experiments suggested such an arrangement.[31] A similar structure was also proposed by Field et al.[32] The first ab initio theoretical investigations were carried out by Hiraoka et al. who used a Hartree−Fock (HF) approach and a limited 3-21G basis set.[39] These authors examined several arrangements where the two benzenes were stacked parallel, perpendicular, side by side in the same plane with their faces parallel, and side by side with their planes perpendicular to each other. Their ground state was a T-configuration where the two benzenes were perpendicular to each other as opposed to the stacked sandwich structure suggested by previous experimental work. The stacked structure was 0.13 eV above this ground state. They further suggested that the difference in energy is small and that the two structures could be considered to be degenerate. As they pointed out, the HF method that does not properly include electron correlations is biased toward symmetry-broken charge-localized structure. They also suggested that a D_{6h} structure would emerge if the correlations were included using configuration interaction or other perturbation techniques. Carrying out configuration interaction on such large systems is computer intensive. In this work, therefore, we use a different approach that employs generalized gradients to include the exchange correlation effects.

It is important to note that a similar situation occurs in neutral benzene dimer where the T-shaped structure and a slipped-parallel structure are found to be nearly degenerate.[21] Recent work has shown that the binding is mainly due to correlation energy and that large basis sets and a proper treatment of correlation are critical to obtaining the correct lowest-energy structures.[94] This is consistent with recent MP2 ab initio calculations on the neutral benzene dimer with a large aug-cc-pVTZ basis set, which showed that the HF binding energies are repulsive.[95] While the situation in the cation is different, the presence of close-lying isomers suggests that a proper inclusion of correlations is vital to the determination of the correct ground state.

To find the ground state of $(C_6H_6)_2^+$, we optimized the geometry of the dimer by starting from several initial geometries where the two benzene rings were stacked parallel, perpendicular with the perpendicular benzene occupying a central or edge position, or the two benzenes in a plane with their C_1-C_4 axes parallel or perpendicular to each other. The total energy was then optimized by calculating the forces on all atoms and allowing atoms to relax in the direction of forces till all the forces dropped below a threshold value of 10^{-4} au. The initial geometries for the T-configuration were obtained using a C_2

(87) Martin, T. P.; Bergmann, T.; Gohlich, H.; Lange, T. *J. Phys. Chem.* **1991**, *95*, 6421.
(88) Wei, S.; Shi, Z.; Castleman, A. W., Jr. *J. Chem. Phys.* **1991**, *94*, 8604.
(89) Ingolfsson, O.; Wodtke, A. M. *J. Chem. Phys.* **2002**, *117*, 3721.
(90) Mackay, A. L. *Acta Crystallogr.* **1962**, *15*, 916.
(91) Farges, J.; Deferaudy, M. F.; Raoult, B.; Torchet, G. *Surf. Sci.* **1985**, *156*, 370.
(92) van de Waal, B. W. *J. Chem. Phys.* **1983**, *79*, 3948.
(93) Dulles, F. J.; Bartell, L. S. *J. Phys. Chem.* **1995**, *99*, 17100.
(94) Tsuzuki, S.; Uchimaru, T.; Sugawara, K.; Mikami, M. *J. Chem. Phys.* **2002**, *117*, 11216.
(95) Sinnokrot, M. O.; Valeev, E. F.; Sherrill, C. D. *J. Am. Chem. Soc.* **2002**, *124*, 10887.

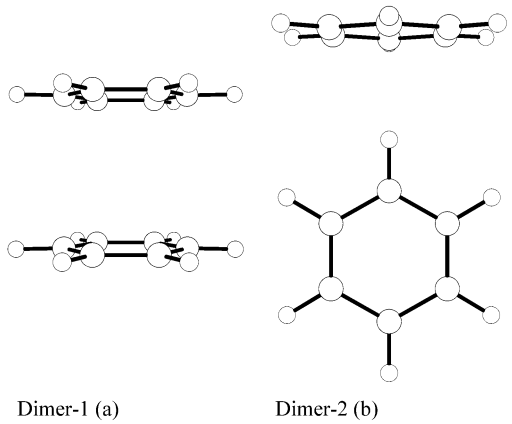

Figure 3. Lowest-energy structures obtained from DFT calculations: (a) stacked sandwich and (b) perpendicular T-shape.

symmetry constraint, while those for the stacked configuration had a D_{6h} symmetry constraint. The final geometries obtained in the symmetry-constraint calculation were slightly perturbed by moving atoms in random directions by a small amount and the calculations were repeated without any symmetry constraint. It was observed that the geometry underwent only a minor relaxation. We found that the dimer is characterized by two nearly degenerate states shown in Figure 3. The stacked configuration is more stable than the T-configuration by only 0.07 eV. It is interesting to note that the various bond lengths in the two geometries are comparable to the corresponding values obtained by Hiraoka et al.[39] using a HF approach. As pointed out earlier, these authors did not include the correlations and the ground-state structures had slightly lower symmetries than obtained in this work. As pointed out by these authors, their symmetry-broken structures are due to a lack of correlation effects and that a more symmetric structure could be obtained once the correlations were included. It is interesting to note that the present calculations that include correlation effects via the DFT do lead to symmetric structures. Also, the stacked configuration is more stable than the T-structure and is the ground state.

3. Monte Carlo Simulations of Benzene Clusters Using the OPLS Potential. Since accurate structural calculations of the benzene cluster cations $(C_6H_6)_n^+$ with $n > 2$ require full consideration of the electron−electron correlations, the calculations of larger clusters would be extremely computer intensive. For these clusters, we chose to employ a MC search technique using the OPLS potential model for benzene to calculate the lowest-energy structures of the clusters. This model reproduces the experimental heat of vaporization, density, heat capacity, and hydration energy with excellent accuracies.[75,96] As described in the Computational Details section, this potential was modified and scaled to reproduce the experimental binding energy of the benzene dimer cation. Figures 4−7 display the structures corresponding to the minima of lowest energies for the $(C_6H_6)_n^+$, $n = 2-6$ clusters. The total cluster configurational energy (E_n), the Coulombic contribution to the configurational energy (E_n^C), the root-mean-square distance between the molecular centers-of-mass in the cluster (R_n), and the ratio of the energy per molecule in the cluster to the energy per molecule in the dimer $[(E_n/n)/(E_n/n)_{n=2}]$ are given in Table 1.

(96) Jorgensen, W. L. *Acc. Chem. Res.* **1989**, *22*, 184.

Table 1. Energies and Structural Parameters for Benzene Cluster Cations $(C_6H_6)_n^+$ with $n = 2-6$[a]

$n(x)$	E_n	E_n/n	E_n^C	E_n^C/n	R_n	E ratio
2(c)	−16.99	−8.49	−1.84	−0.92	2.58	1.00
3(d)	−34.00	−11.33	−3.56	−1.19	3.65	1.33
3(e)	−31.73	−10.58	−6.16	−2.05	3.45	1.25
4(f)	−49.32	−12.33	−7.62	−1.91	3.72	1.45
4(g)	−49.10	−12.28	−7.45	−1.86	3.72	1.45
4(h)	−46.72	−11.68	−9.69	−2.42	3.73	1.38
5(i)	−64.78	−12.96	−10.88	−2.18	3.81	1.53
5(j)	−64.11	−12.82	−11.51	−2.30	4.16	1.51
5(k)	−54.23	−10.85	−11.76	−2.35	3.89	1.28
6(l)	−80.59	−13.43	−14.88	−2.48	4.15	1.58
6(m)	−79.76	−13.29	−14.98	−2.50	4.23	1.57

[a] x denotes the isomer structure shown in Figures 4−7. E_n is the total cluster configurational energy, E_n^C is the Coulombic contribution to the configurational energy, and R_n is the root-mean-square distance between the molecular centers-of-mass. The E-ratio $[(E_n/n)/(E_n/n)_{n=2}]$ gives the ratio of the energy per molecule to the energy per molecule in the dimer. Energies in kcal/mol, R_n in Å.

For $(C_6H_6)_2^+$ we have the sandwich structure (Dimer-3 (c) in Figure 4) skewed by 30° to optimize electrostatic interactions. This is a little different from the DFT structure (Dimer-1 (a), Figure 3), which has the eclipsed parallel configuration. The molecular centers-of-mass (COM) are separated by 3.65 Å in the MC structure (c) as compared to 3.50 Å in the DFT structure (a).

For the trimer $(C_6H_6)_3^+$, two isomers were found as shown by structures (d) and (e) in Figure 4. Isomer (d) has a triple-stack structure with the same 30° skewing as in the dimer. The distance between each of the neutral benzene molecular COM and the cluster COM (d_{COM}) is 3.65 Å, with the benzene cation located at the cluster COM. For the second isomer, structure (e), we have a quasi-planar triangular structure with the angles between the three molecular planes (φ) as 142, 122, and 96° (rather than all φ values at 120°). In structure (e) the cation is closest to the cluster COM with a d_{COM} value of 2.10 Å, with the two neutral molecules at 2.86 and 3.36 Å. The plane of each molecule is nearly perpendicular to the plane containing all three molecular centers-of-mass.

For $(C_6H_6)_4^+$, three isomers (f, g, and h) were located as shown in Figure 5. Isomer (f) has the structure of the $(C_6H_6)_3^+$ isomer (d) with an additional neutral molecule resting against the side of the pancake-like trimer stack. The cation is again closest to the cluster COM with a d_{COM} value of 1.61 Å, with the neutral molecules at 3.36 Å (1) and 3.72 Å (2). The second isomer of $(C_6H_6)_4^+$ [structure (g)] differs only slightly from structure (f). The third isomer [structure (h)] can be viewed as a distorted tetrahedron. Instead of all φ values at 109.5° and all d_{COM} values equal (perfect tetrahedron), the φ values in structure (h) range from 86 to 118° and the d_{COM} values range from 2.18 to 3.67 Å, with the cation again closest to the cluster COM.

For $(C_6H_6)_5^+$ and $(C_6H_6)_6^+$ clusters, three (i, j, and k), and two (l and m) isomers, respectively, were located as shown in Figures 6 and 7, respectively. Isomer (i) of $(C_6H_6)_5^+$ continues the growth pattern of isomer (f) by adding a second molecule on the side of the pancake-stack trimer. The cation is again closest to the cluster COM with a d_{COM} value of 1.94 Å, with the neutral molecules having values in the range 3.59−3.76 Å. Isomer (j) of $(C_6H_6)_5^+$ is a variant of isomer (i). The main difference between isomers (i) and (j) is that the pancake-stack trimer in (i) is surrounded by two molecules located along the sides of the trimer stack (the cation is perpendicular to one of the side molecules). However, in isomer (j) there are three

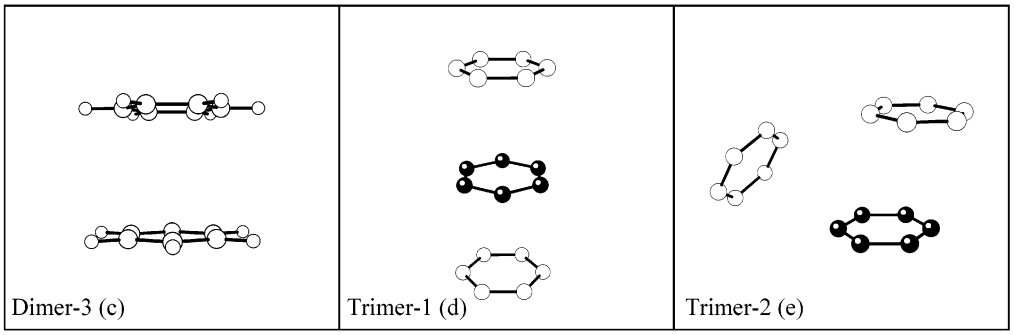

Figure 4. Lowest-energy structures obtained from MC pair potential calculations: (c) dimer-3; (d) trimer-1, and (e) trimer-2. Energies are given in Table 1.

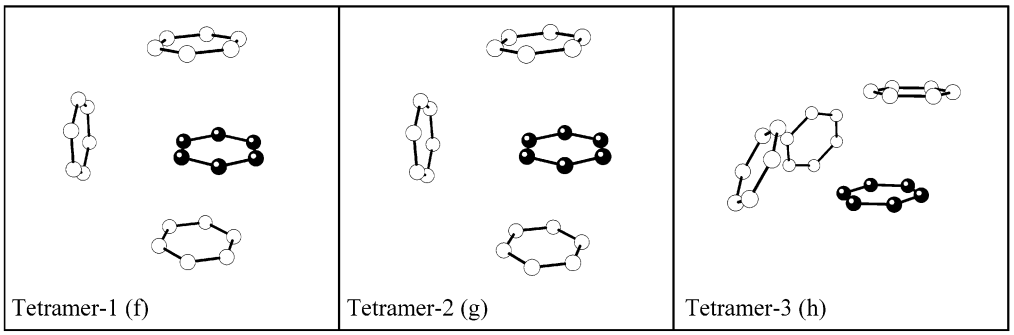

Figure 5. Lowest-energy structures obtained from MC pair potential calculations: (f) tetramer-1, (g) tetramer-2, and (h) tetramer-3. Energies are given in Table 1.

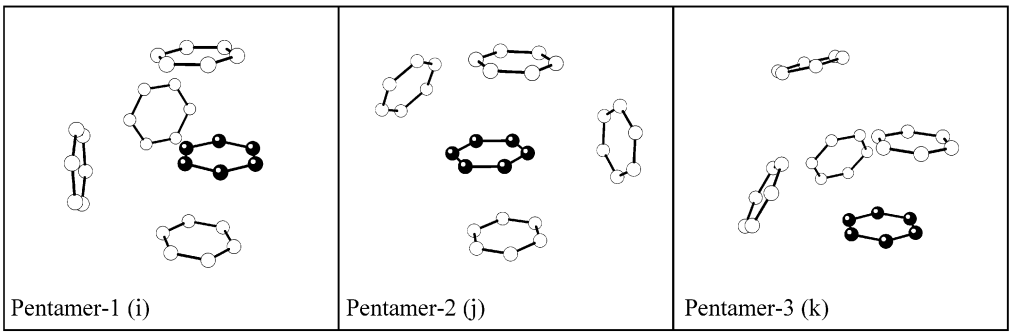

Figure 6. Lowest-energy structures obtained from MC pair potential calculations: (i) pentamer-1, (j) pentamer-2, and (k) pentamer-3. Energies are given in Table 1.

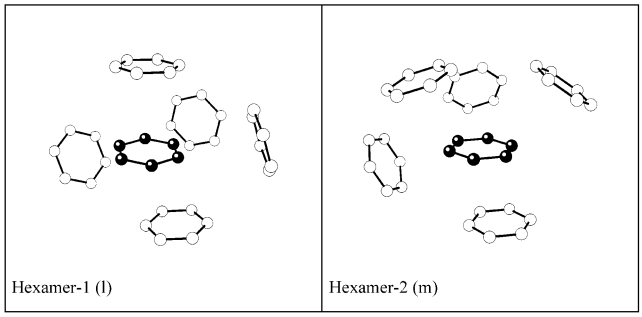

Figure 7. Lowest-energy structures obtained from MC pair potential calculations: (l) hexamer-1, and (m) hexamer-2. Energies are given in Table 1.

molecules above and one molecule below the cation plane. This arrangement results in a less compact structure for isomer (j) as compared to isomer (i). This is clearly reflected in the R_n values (R_n is a measure of cluster radius according to eq 5) of 4.16 and 3.81 Å calculated for isomers (j) and (i), respectively. The higher-energy isomer (k) [about 16% higher in energy than isomer (i) as shown in Table 1] is irregular with all d_{COM} values lie in the range 3.11−3.86 Å, with the cation still closest to the cluster COM. The R_n value for isomer (k) is 3.89 Å, between the values corresponding to isomers (j) and (i).

For the $(C_6H_6)_6^+$ cluster, isomer (l) continues the lowest-energy isomer pattern by adding a third molecule around the central pancake-stack trimer as shown in Figure 7. The cation is 1.52 Å from the cluster COM, with the neutral molecules at distances of 3.49−4.78 Å. Isomer (m), shown in Figure 7, is a variant of isomer (l) but can be viewed as a continuation of the alternative growth sequence noted above for the higher-energy isomers of the $n = 2-5$ clusters, as well as a continuation of the lowest-energy isomer pattern.

With the strong $B \leftrightarrow B^+$ interaction (17 kcal/mol),[33] one would expect to find as many neutral benzenes coordinated closely to the cation as possible. Yet, in the present results, one finds two prominent growth patterns: one involves a dimer cation core, and the other involves a stacked trimer core. The lowest-energy isomers of the $n = 3-6$ clusters incorporate the pancake trimer stack as the cluster's core. Comparisons of the

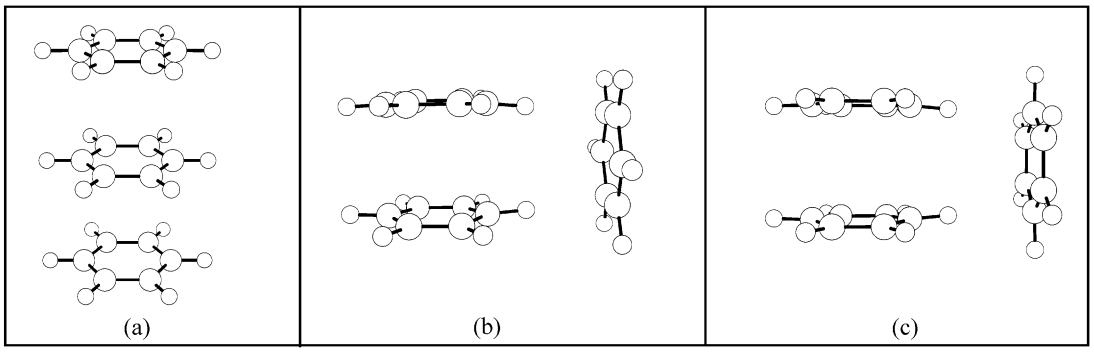

Figure 8. Lowest-energy structure obtained from DFT calculations on $(C_6H_6)_3^+$. (a) Stacked, ground-state structure with a binding energy of 1.22 eV. (b) Perpendicular, higher-energy isomer with a binding energy of 1.07 eV, and (c) perpendicular, higher-energy isomer with a binding energy of 0.98 eV. All binding energies are calculated with respect to dissociation to a benzene radical cation and two neutral benzene molecules.

calculated collision cross sections corresponding to these structures with the experimentally determined cross sections of $(C_6H_6)_n^+$ with $n = 2-6$, will provide a basis for confidence in using the modified OPLC potential with the MC search procedure to obtain reliable structures for larger charged benzene clusters. These comparisons are presented in the next section.

4. DFT Structures of Benzene Trimer Cation. To provide a further check on the reliability of the modified OPLC potential in obtaining accurate structures of larger benzene cluster cations, we carried out DFT calculations on $(C_6H_6)_3^+$ in stacked and perpendicular configurations. In the stacked configuration, the three benzene units were stacked parallel to each other. To make the calculations feasible, minimal symmetry constraints corresponding to reflections in the *xy*, *yz*, and *xz* planes were imposed. For the perpendicular case we examined two different arrangements. In each case, two benzene units were stacked parallel to each other. The third benzene was arranged perpendicular to the stacked benzenes. The two perpendicular configurations differed in the arrangement of the third benzene. In one case, the H atoms of the stacked benzenes pointed toward the middle of the C−C bond of the perpendicular benzene. In the second case, the H atoms of the two-stacked benzenes pointed toward the C atoms of the perpendicular benzene. In the perpendicular cases, the symmetry operations corresponded to reflections in *xz* and *xy* planes. The energies were optimized by varying the remaining degrees of freedom and the resulting structures are shown in Figure 8. The ground state corresponds to the stacked configuration (Figure 8-a) with a binding energy of 1.22 eV with respect to dissociation to a benzene radical cation and two neutral benzene molecules. The perpendicular configurations (Figure 8, b and c) were respectively 0.15 and 0.24 eV above the ground state. The ground-state structure (Figure 8-a) is similar to the lowest-energy structure obtained from the MC calculations (trimer-1 (d) displayed in Figure 4). Furthermore, the second lowest-energy isomers obtained from both the DFT and MC calculations are similar. These results provide support for using the MC approach to obtain reliable lowest-energy structures of with $(C_6H_6)_n^+$ $n = 3-6$.

5. Mobilities of Benzene Cluster Cations. Figure 9 shows a typical ATD of the mass-selected dimer $(C_6H_6)_2^+$ injected into 2.5 Torr helium in the drift cell at room temperature using a 50 μs ion gate pulse. A single, relatively sharp peak is observed. The inset in Figure 9 shows a plot of t_d vs P/V used to calculate the mobility of $(C_6H_6)_2^+$ according to eq 3. The excellent linear correlation in the data indicates that under the low-field regime employed in our measurements (E/N < 5.0

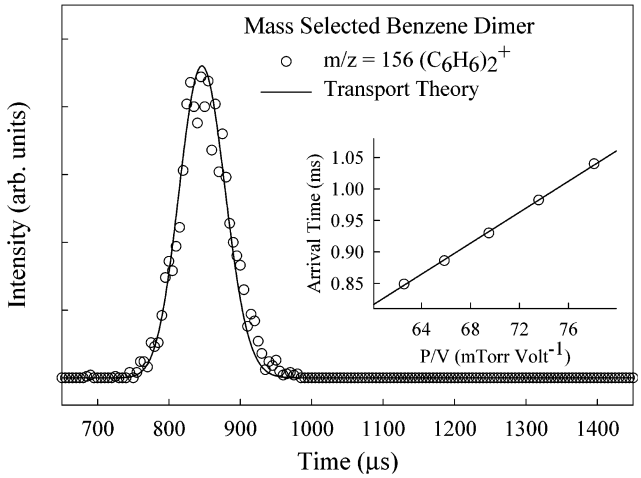

Figure 9. Comparison of the measured ATD of the benzene dimer cation $(C_6H_6)_2^+$ with the prediction of transport theory (eq 6). The inset shows the linear plot of t_d vs P/V used to calculate the mobility.

Td), the ion's drift velocity is small compared to the thermal velocity, and the ion mobility is independent of the field strength. The repeated mobility measurements yield a reduced mobility for the benzene dimer cation at 303 K of $K_0 = 7.6 \pm 0.1$ (0.2) $cm^2 \cdot V^{-1} \cdot s^{-1}$, the uncertainty given here is ± 1 standard deviation in the repeated measurements, the value in parentheses represents a 3% experimental error in the mobility measurements. Our result is in excellent agreement with the reported reduced mobility of $(C_6H_6)_2^+$ ($K_0 = 7.6 \pm 0.3$ $cm^2 \cdot V^{-1} \cdot s^{-1}$) measured by Krishnamurthy et al. using a selected-ion flow-drift tube apparatus.[71]

The measured ATD can be calculated from the transport equation for a short packet (delta pulse) of ions injected into a cylindrical drift tube through an aperture of area a using eq 6.[48,49]

$$\phi(t) = \frac{sae^{-\alpha t}}{4\sqrt{\pi D_L t}}\left(v_d + \frac{l}{t}\right)\left(1 - \exp\left(-\frac{r_0^2}{4D_T t}\right)\right) \exp\left(-\frac{(l - v_d t)^2}{4D_L t}\right) \quad (6)$$

The ions are introduced as a delta pulse in the form of an axially thin disk of radius r_0 and uniform surface density s. Loss of ions through reactions during the drift time can be accounted for through the frequency factor α. D_L and D_T are the longitudinal and transverse diffusion coefficients, which (under

Table 2. Measured and Calculated Reduced Mobility (K_0/$cm^2 \cdot V^{-1} \cdot s^{-1}$) and Collision Cross Section in Helium (Ω/Å^2) for the Benzene Cluster Cations $(C_6H_6)_n^+$ with $n = 2-6$[a]

	calculatedst		experimental				% difference	
	Ω	K_0	Ω	% abundance	K_0	$K_{0(av)}$	Ω	K_0
dimer-1 (a)	72.9	7.4	71.2		7.6		2.4	2.6
dimer-2 (b)	77.4	7.0					8.7	7.9
dimer-3 (c)	73.7	7.3					3.5	3.9
trimer-1 (d)	100.2	5.4	101.1	46.3	5.3	5.5	0.9	1.9
trimer-2 (e)	98.1	5.5	94.2	53.7	5.7		4.1	3.5
tetramer-1 (f)	118.9	4.50	118.8	32.2	4.5	4.7	0.1	0.0
tetramer-2 (h)	117.9	4.54	111.5	67.8	4.8		5.7	5.4
pentamer-1 (i)	133.1	4.0	131.6	46.7	4.1	3.9	1.1	2.4
pentamer-2 (j)	140.3	3.8	141.6	53.3	3.8		1.0	0.0
hexamer-1 (l)	149.8	3.6	144.0	56.5	3.7	3.6	4.0	2.7
hexamer-2 (m)	153.3	3.5	154.5	43.5	3.5		0.8	0.0

[a] The mobilities and % abundance obtained from fitting the measured ATD of each of the $n = 3-6$ clusters to two isomers are given under Experimental Section. K_0 (av) is the average mobilities obtained from the linear fits shown in Figure 11-b, assuming one isomer for each cluster. The cross sections are calculated using the trajectory method (see ref 97).

low-field conditions) are related to the mobility by the Einstein equation:[49]

$$D_L = D_T = K\frac{k_B T}{ze} \tag{7}$$

where *ze* is the number of charges times the charge of the electron.

A comparison of the measured ATD of the $(C_6H_6)_2^+$ ions with the prediction from transport theory using eq 6 is shown in Figure 9. From the excellent agreement with the predicted peak shape, we conclude that either only one isomer is present in the $(C_6H_6)_2^+$ mass channel or, if there are multiple isomers, they have essentially identical collision cross sections. However, it should be pointed out that two structures with different cross sections could result in a single sharp ATD peak if the two structures rapidly interconvert on the time scale of the experiment. For example, a 90° flip of the benzene molecule in the stacked dimer-1 (a), would produce the perpendicular T-shape dimer-2 (b) shown in Figure 3.

According to the kinetic theory,[49] eq 8 relates the mobility of an ion to the average collision cross section of the ion with the buffer gas.

$$K = \frac{1}{N}\frac{(18\cdot\pi)^{1/2}}{16}\left[\frac{1}{m}+\frac{1}{m_b}\right]^{1/2}\frac{z\cdot e}{(k_B\cdot T)^{1/2}\cdot\Omega^{(1,1)}_{av}} \tag{8}$$

N is the buffer gas number density, *m* is the mass of the ion, m_b is the mass of a buffer gas atom, *z* is the number of charges *e* is the electron charge, k_B is Boltzmann's constant, and $\Omega^{(1,1)}_{av}$ is the average collision integral.

The measured mobilities are used to calculate average Ωs for the $(C_6H_6)_n^+$ ions in helium using eq 8, and the resulting values are listed in Table 2. The lowest-energy structures of the benzene dimer cation obtained from the DFT calculations (structures a and b in Figure 3) and the pair-potential MC technique (structure c in Figure 4), are used to obtain average collision cross sections using the trajectory calculations which employ a potential consisting of LJ and ion-induced dipole interactions.[60,97,98] The calculated cross sections and mobilities, shown in Table 2, indicate that the lowest-energy stacked structure predicted by the DFT calculation results in an average cross section that compares very well (2.4%) with the experimentally determined value. Also, the dimer structure obtained from the MC calculations [structure (c) in Figure 4] yields a reasonable agreement (within 3.5%) with the measured cross section. The difference is clearly due to the 30° rotation angle of one of the parallel molecular planes with respect to the other in structure (c). The good agreement between the cross section calculated for the DFT lowest-energy dimer structure and the experimental value indicates that the two benzene rings in the dimer cation are nearly eclipsed as in the perfect sandwich structure (a). On the other hand, the cross section of the T-configuration differs significantly (8.7%) from the measured cross section. If the interconversion between the two structures were effective, one would expect the measured cross section to be an average of the cross sections of the two structures. Since the measured cross section is within 2.4% of the calculated cross section of the sandwich structure, it can be concluded that the $(C_6H_6)_2^+$ adopts the stacked parallel configuration (or spends more of its lifetime exhibiting the parallel rather than the perpendicular configuration) in agreement with the ground-state structure calculated by the DFT.

The mobilities of the larger clusters $(C_6H_6)_n^+$ with $n = 3-6$ were measured in the same way described above for the dimer experiments [50 μs ion gate width and low field regime (E/N < 5 Td) at room temperature (303 K)]. However, because the signal intensity of the cluster species decreases with increasing size (see Figure 2), mass-selection in the first quadrupole could not produce a practical level of signal sufficient for the mobility experiments. Therefore, for the $n = 3-6$ clusters, the first quadrupole was operated in an *RF-only* mode, where a range of cluster ions above a selected *m*/*z* value is allowed to pass through the quadrupole, and subsequently injected into the drift tube. The selected *m*/*z* values of the first quadrupole for the $n = 3-6$ clusters were 234, 312, 390, and 468, respectively. By setting the first quadrupole at the *m*/*z* value corresponding to a particular cluster (*n*) and scanning the second quadrupole, we found that the ion distribution exiting the drift cell was mostly (more than 90%) due to the *n* cluster and only a small fraction (less than 10%) due to the $(n + 1)$ cluster. In all the mobility experiments the second quadrupole was operated in a single-ion mode to measure the ATD of a particular cluster ion of interest.

To investigate the effects of cluster ion fragmentation at the entrance of the drift tube, we measured the ATDs of the benzene dimer and monomer ions following the injection of a mass-selected dimer ion at different injection energies. The results, shown in Figure 10, indicate that with injection energies (E_{CM}, center of mass kinetic energies)[99] of 0.25 and 0.50 eV, 72 and 94%, respectively, of the mass-selected $(C_6H_6)_2^+$ ions fragment into $C_6H_6^+$. However, the measured mobility of the $C_6H_6^+$ ions fragmented from $(C_6H_6)_2^+$ (11.7 $cm^2/V\cdot s$) is similar, within the uncertainty of the measurements, to the measured mobility of mass-selected $C_6H_6^+$ ions (11.5 $cm^2/V\cdot s$). Furthermore, both the ATDs of the $C_6H_6^+$ ions dissociated from $(C_6H_6)_2^+$ and the mass-selected $C_6H_6^+$ ions show excellent agreement with the predicted ATD from transport theory according to eq 6. This

(97) Mesleh, M. F.; Hunter, J. M.; Shvartsburg, A. A.; Schatz, G. C.; Jarrold, M. F. *J. Phys. Chem.* **1996**, *100*, 16082.
(98) Shvartsburg, A. A.; Hudgins, R. R.; Dugourd, P.; Jarrold, M. F. *J. Phys. Chem. A* **1997**, *101*, 1684.
(99) Armentrout, P. B. *J. Am. Mass Spectrom.* **2002**, *13*, 419.

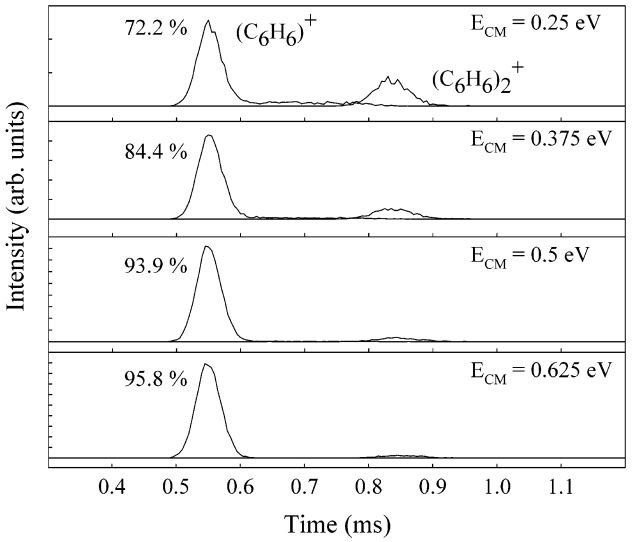

Figure 10. Effect of injection energy on the dissociation of mass-selected $(C_6H_6)_2^+$ ions.

indicates that the fragmentation of the dimer ion takes place at the entrance to the cell and has no effect on the measured mobility of the generated monomer ion or on the ATD peak shape. Considering the relatively large binding energy of the dimer cation, it is most likely that larger clusters with less binding energy than the dimer would dissociate at the entrance of the drift tube, thus creating a new distribution of smaller clusters. Also, the ATD and mobility of the $(C_6H_6)_2^+$ ions measured with the first quadrupole operating in the *RF-only* mode are identical to those measured with the mass-selection mode. These results indicate that the use of the *RF-only* mode for the injection of larger clusters into the drift has no serious effects on the measured mobilities of larger clusters.

Figure 11-a displays typical ATDs of the $(C_6H_6)_n^+$ ions for $n = 1-6$, and Figure 11-b shows the corresponding plots of t_d vs P/V used to calculate the mobilities of $(C_6H_6)_n^+$ according to eq 3 and assuming that the ATD peak contains only one structure. As shown below, the ATDs of the $n = 3-6$ clusters are analyzed in terms of two structural isomers for each cluster. Therefore, the mobilities obtained from the t_d vs P/V plots shown in Figure 11-b represent average mobilities of the two structural isomers for each cluster. These average mobilities (K_{av}) are listed in Table 2.

Comparison of the measured ATDs of the $(C_6H_6)_n^+$ ions with $n = 1-6$ to those calculated from the transport equation (eq 7) can be used to ascertain whether the observed features result from several isomers with slightly different mobilities or appear to result from only a single isomer as in the case of $(C_6H_6)_2^+$ ions shown in Figure 9. Comparison of the ATDs of $(C_6H_6)_3^+$ indicates that the measured distribution is considerably broader than the calculated ATD from eq 6, as shown in Figure 12-a. The broader distribution indicates that the $(C_6H_6)_3^+$ clusters do not have a single structure in the gas phase, but exist in a number of closely related conformations. However, the possibility of dissociation of the larger clusters inside the drift tube may also result in broader distributions of the $(C_6H_6)_3^+$ ions. To further determine whether the measured ATDs of the $(C_6H_6)_3^+$ ions are influenced by dissociation inside the drift tube, we changed the buffer gas pressure and the drift voltage so that the ions spend either more (higher pressure or lower drift voltage) or less time (lower pressure or higher drift voltage) in the drift tube. If the ions spend more time inside the drift tube, dissociation from larger clusters should result in significant tails in the ATDs compared to the calculated ones. In contrast, the experiments showed that the ATDs of the $(C_6H_6)_n^+$ ions with $n = 3-6$ remain symmetric with no obvious tailing at smaller drift fields which correspond to longer drift times. These results further support the conclusion that fragmentation of the cluster ions takes place at the entrance of the drift tube, and that no significant dissociation takes place during the drift time. Therefore, the observed broader distribution of the $(C_6H_6)_3^+$ ions appears to reflect the existence of more than one isomer with close collision cross sections. In fact, the MC calculations, discussed in section 3, found two isomers for the $(C_6H_6)_3^+$ cluster [structures (d) and (e) in Figure 4] with less than 7% difference in energy. These structures are used to obtain average collision cross sections using the trajectory calculations.[60,97] The calculated cross sections and mobilities, shown in Table 2,

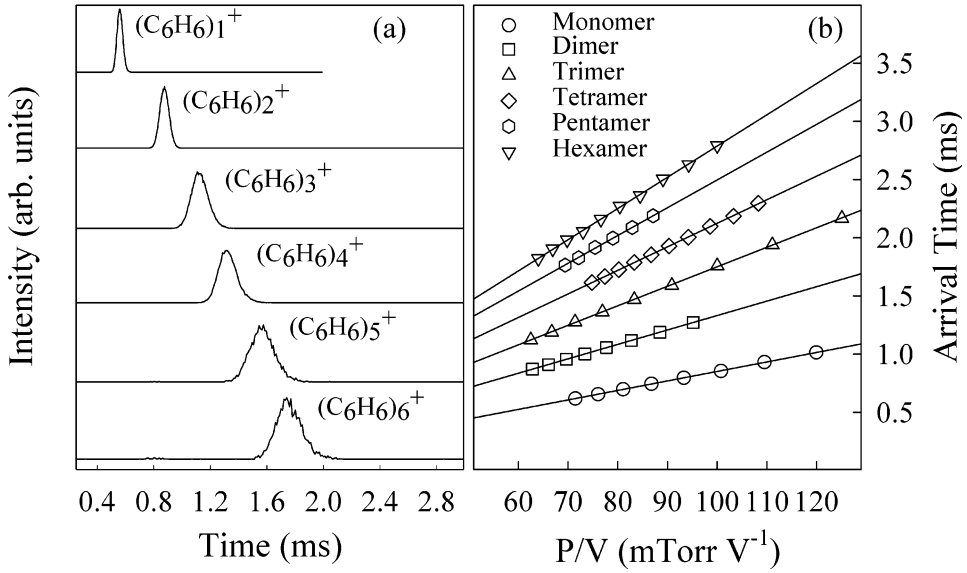

Figure 11. (a) Measured ATDs of $(C_6H_6)_n^+$ with $n = 1-6$. (b) Plots of t_d vs P/V used to calculate average mobilities [K_0 (av)] of the $(C_6H_6)_n^+$ with $n = 1-6$, assuming a single isomer for each cluster.

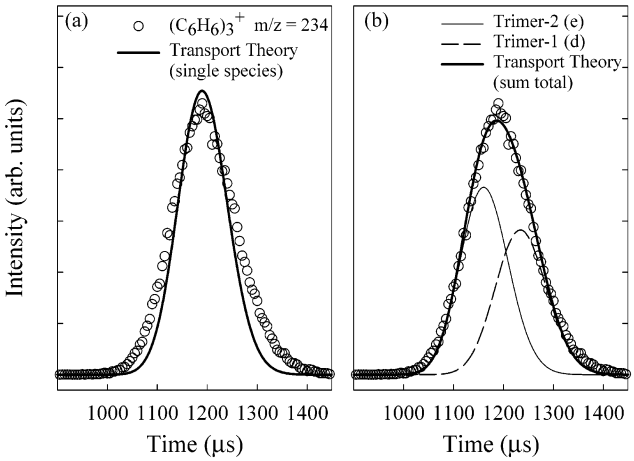

Figure 12. (a) Comparison of the measured ATD of the benzene trimer cation $(C_6H_6)_3^+$ with the predictions of transport theory for a single isomer. (b) Comparison of the measured ATD of the benzene trimer cation $(C_6H_6)_3^+$ with the predictions of transport theory for two structural isomers.

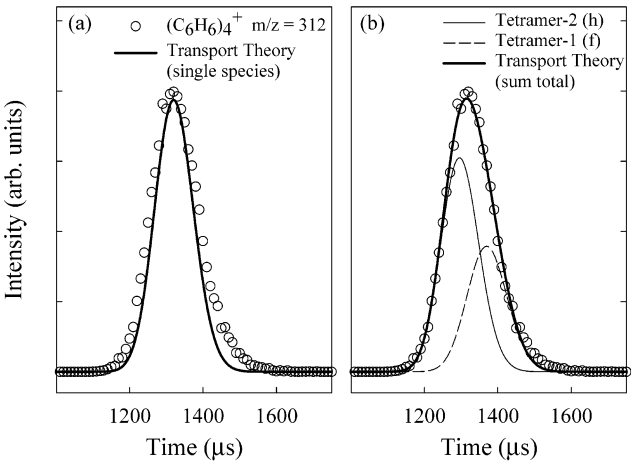

Figure 13. (a) Comparison of the measured ATD of the benzene tetramer cation $(C_6H_6)_4^+$ with the predictions of transport theory for a single isomer. (b) Comparison of the measured ATD of the benzene tetramer cation $(C_6H_6)_4^+$ with the predictions of transport theory for two structural isomers.

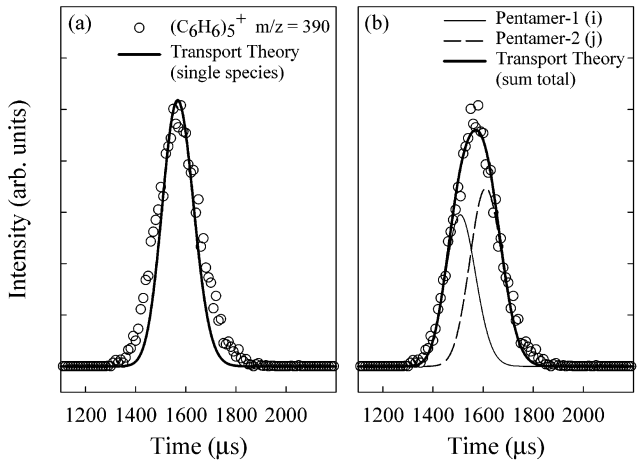

Figure 14. (a) Comparison of the measured ATD of the benzene pentamer cation $(C_6H_6)_5^+$ with the predictions of transport theory for a single isomer. (b) Comparison of the measured ATD of the benzene pentamer cation $(C_6H_6)_5^+$ with the predictions of transport theory for two structural isomers.

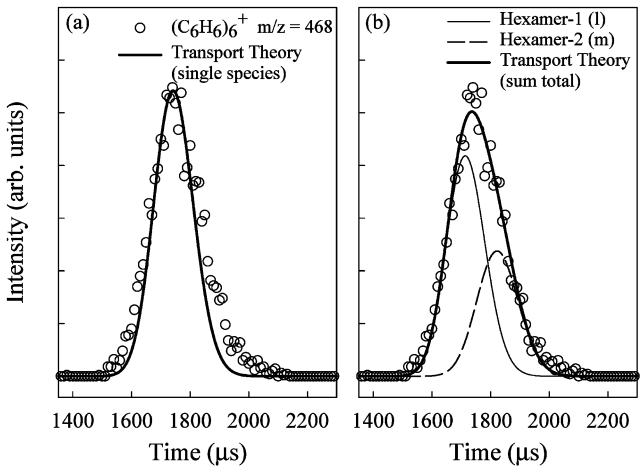

Figure 15. (a) Comparison of the measured ATD of the benzene hexamer cation $(C_6H_6)_6^+$ with the predictions of transport theory for a single isomer. (b) Comparison of the measured ATD of the benzene hexamer cation $(C_6H_6)_6^+$ with the predictions of transport theory for two structural isomers.

indicate that the two lowest-energy isomers identified by the MC search technique result in average cross sections that compare well with the measured Ω for the $(C_6H_6)_3^+$ cluster [the mobilities of structures (d) and (e) differ by 1.9 and 3.5%, respectively, from the mobilities of $(C_6H_6)_3^+$ obtained from the ATD fits to two isomers with the % abundance given in Table 2].

Similar to the $(C_6H_6)_3^+$ ions, the ATDs of $(C_6H_6)_n^+$ with $n = 4-6$, consist of broader distributions as compared to the calculated distributions from the transport equation as shown in Figures 13−15. Further support that the broad ATDs of the $(C_6H_6)_n^+$ ions with $n = 3-6$, reflect the existence of several structural isomers for each cluster is obtained by measuring the fwhm of the ATDs at increasing resolutions of the mobility tube. The results of these experiments indicate that increasing the resolving power (by increasing both the drift field and the helium pressure but keeping P/V constant in order to keep the mobilities in the low-field limit) results in larger fwhms of the ATD peaks as compared to the calculated distributions. Our current drift tube has a resolving power of about 20; thus, isomers with more than 5% difference in cross sections can be separated. With high-resolution drift tubes (resolving power of 200−300),[100] it would be possible to separate the broad ATDs of larger of $(C_6H_6)_n^+$ to resolved components corresponding to families of structural isomers with very close (less than 5%) collision cross sections. Another possibility to improve the resolution is to carry out the mobility experiments at lower temperatures since the resolution depends on $T^{-1/2}$.[100] Future experiments will investigate the temperature dependence of the mobilities of $(C_6H_6)_n^+$. It would be interesting to observe structural changes at different temperatures, which can yield quantitative information on the isomerization barriers between different structural isomers.

The measured ATD of the $(C_6H_6)_4^+$ clusters can be fitted to two structural isomers as shown in Figure 13-b. The resulting mobilities, cross sections and % abundance are given in Table 2. The calculated lowest-energy structures (f, g, and h in Figure 5) indicate that structures (f) and (g) are nearly similar with only 0.2 kcal/mol difference in energy. These structures are assigned to the first isomer of the $(C_6H_6)_4^+$ cluster. The calculated cross section of these structures agree perfectly with

(100) Dugourd, P.; Hudgins, R. R.; Clemmer, D. E.; Jarrold, M. F. *Rev. Sci. Instrum.* **1997**, *68*, 1122.

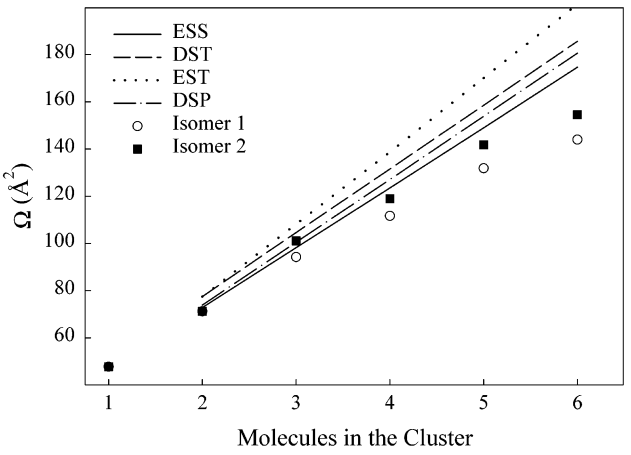

Figure 16. Comparison of the measured collision cross sections Ω (Å^2) for $(C_6H_6)_n^+$ with the cross sections calculated for the ESS, DST, EST, and DSP structural patterns. The points for isomer 1 and 2 are obtained from the ATD fits to two peaks (see text for details).

the measured cross section assigned to one of the two structural isomers used to fit the ATD of $(C_6H_6)_4^+$ shown in Figure 13-b. The next lowest-energy structure (structure h in Figure 5) results in a cross section that agrees within 5.7% with the measured cross section assigned to the second isomer of the $(C_6H_6)_4^+$ cluster. Clearly the agreement is not as good as for the lowest-energy structure (structure f). This is probably an indication that the frozen structure used to calculate the collision cross section of the second isomer of $(C_6H_6)_4^+$ does not reflect the dynamic nature of collision process. In this case, molecular dynamic simulations may obtain a better description of the structure involved in calculating the collision cross section where an average of several conformations of the cluster isomer can be considered.[69,70]

The two lowest-energy isomers of the $(C_6H_6)_5^+$ cluster (structures i and j in Figure 6) result in cross sections that agree within 1% with the cross sections obtained from the fitting of the ATD to two isomers as shown in Figure 14-b. Similarly, the two lowest-energy structures of the $(C_6H_6)_6^+$ cluster (structures l and m in Figure 7) reproduce the cross sections obtained from fitting the ATD to two isomers as shown in Figure 15-b. The resulting mobilities, cross sections, and % abundance are given in Table 2.

From the above results, it is clear that the cross sections calculated for the lowest-energy isomers located by the MC quenching technique provide very good matching to the measured ATDs as shown in Figures 13−15 and Table 2. With the exception of the second isomer of the $(C_6H_6)_4^+$ cluster [structure (h)], the differences between the measured and calculated cross sections are less than 4%.

Figure 16 shows the average collision cross section obtained from the measured mobility of each of $(C_6H_6)_n^+$ ions, as a function of the number of benzene molecules in the cluster. The smoothly increasing function of the cluster size is expected for structurally closely related cluster ions. The measured cross sections for $n = 2-6$ are compared to the cross sections corresponding to the four idealistic growth patterns ESS, DSP, EST, and DST considered for the assembly of benzene cluster cations. The ESS and EST patterns are created by duplicating the sandwich and T-shaped dimer structures, respectively obtained from the DFT calculations. The DSP structure is obtained by sequentially sliding each benzene ring in the parallel configuration by 50% from the eclipsed position. The DST structure is constructed by duplicating the T-shaped configuration in a displaced pattern.

The eclipsed sandwich stacked pattern is characterized by compact structures and, therefore, exhibits the smallest cross sections and shows a smaller increase in cross sections as cluster size increases. The eclipsed staked T-shaped structures show the largest cross sections and the largest increase with cluster size. It is clear that the measured cross sections for $n = 2$ and 3 lie very close to the ESS growth pattern. However, a significant deviation from the ESS pattern starts to appear at $n = 4$, and becomes more apparent at $n = 5$ and 6. This indicates that the perfect sandwich structures with all the molecules stacked parallel to one another are less likely to be present in larger clusters. It is also expected that the number of lowest-energy isomers will increase rapidly with n. Figure 16 highlights the value of the ion mobility experiments where a hypothetical structural pattern can be tested through the comparison with the measured cross sections. For example, if it is possible to assemble multiple phenyl rings through appropriate covalent linkages to produce a stacked structure, then one can measure the cross section of such an assembly and obtain direct information on the degree of stacking. This in turn, would guide the synthesis approach by optimizing the experimental parameters needed for the design of new molecular assemblies. Future studies will focus on the application of ion mobility to obtain direct structural information on the assemblies of organic molecules including oligomers of olefin and diolefin molecules.

V. Conclusions

In this work we used gas-phase ion mobility experiments and theoretical calculations to determine the structures of benzene cluster cations $(C_6H_6)_n^+$ with $n = 2-6$. Density functional calculation, at an all-electron level and without any symmetry constraint, predicts that the dimer cation has two nearly degenerate ground-state structures with the sandwich configuration more stable than the T-configuration by only 0.07 eV. The ion mobility experiment indicates that only one structure is observed for the mass-selected dimer cation at room temperature. The calculated cross section for the sandwich structure agrees very well with the experimental value. For the $n = 3-6$ clusters, the experiments suggest the presence of at least two structural isomers with close cross sections for each cluster. The calculated cross sections for the two lowest-energy isomers of each cluster predicted by Monte Carlo simulations agree well with the experimental results. The clusters' structures reveal two different growth patterns involving a sandwich dimer core or a pancake trimer stack core. The trimer stack allows the charge to hop between two dimers, thus maximizing charge resonance interaction in the clusters. The lowest-energy isomers of the $n = 3-6$ clusters incorporate the pancake trimer stack as the cluster's core.

The present work also reports the first observation of magic numbers larger than $n = 14$ in the $(C_6H_6)_n^+$ cluster sequence. The observation of enhanced ion intensities at $n = 20$, 24, 27, and 30 is consistent with the incorporation of a benzene dimer cation within a double icosahedral ($n = 20$) and other interpenetrating icosaherdral structures ($n = 24$, 27, and 30),

indicating that the stacked dimer cation becomes the predominant ion core in larger clusters.

On the basis of the ion mobility results and the structural calculations, the stacked motif (dimer and trimer) among charged aromatic−aromatic interactions is expected to influence the structures of molecular systems containing multiple aromatic components. For smaller systems (4−6 aromatic rings), the stacked trimer is expected to occupy the central core, while for larger systems the dimer cation becomes the predominant core. This conclusion may provide new insights for experimental and theoretical studies of molecular design and recognition involving aromatic systems.

Acknowledgment. It is a pleasure to acknowledge invaluable discussions with Drs. M. T. Bowers, M. F. Jarrold, D. E. Clemmer, and P. R. Kemper regarding the ion mobility technique. We gratefully acknowledge financial support from the National Science Foundation (CHE- 9816536).

JA035504M